Mechanical and thermomechanical characterisation of vacuum-infused thermoplastic- and thermoset-based composites

Winifred Obande [a], Dimitrios Mamalis [a], Dipa Ray [a,*], Liu Yang [b], Conchúr M. Ó Brádaigh [a]
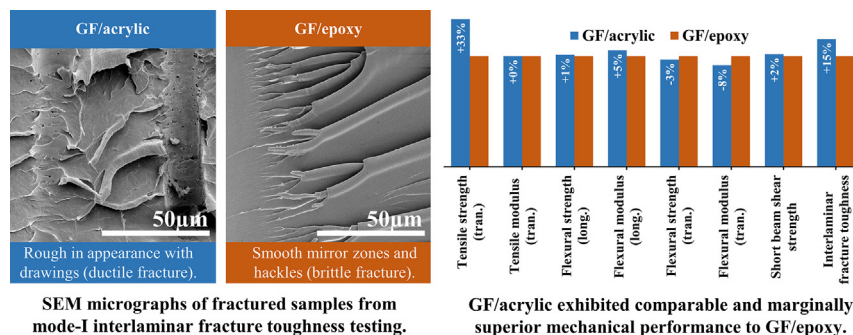
[a] School of Engineering, Institute for Materials and Processes, The University of Edinburgh, Sanderson Building, Robert Stevenson Road, Edinburgh EH9 3FB, Scotland, United Kingdom
[b] University of Strathclyde, Department of Mechanical and Aerospace Engineering, 75 Montrose Street, Glasgow G1 1XJ, United Kingdom

HIGHLIGHTS

- An in-situ polymerised thermoplastic acrylic composite was manufactured by liquid resin infusion.
- The mechanical and thermomechanical characteristics of the acrylic material have been benchmarked against an epoxy reference.
- The acrylic composite exhibited superior tensile (90°), flexural (0°), interlaminar shear and fracture toughness properties.
- "Thermomechanical characterisation revealed marked superiority in the damping behaviour of the acrylic composite.

GRAPHICAL ABSTRACT

SEM micrographs of fractured samples from mode-I interlaminar fracture toughness testing.

GF/acrylic exhibited comparable and marginally superior mechanical performance to GF/epoxy.

ARTICLE INFO

ABSTRACT

In this work, a comparative performance study was conducted on glass fibre-reinforced thermoplastic acrylic and thermosetting epoxy laminates produced by vacuum-assisted resin transfer moulding. Mechanical characterisation revealed that the acrylic-based composite had superior transverse tensile strength and mode-I fracture toughness to the epoxy composite, while longitudinal flexural properties and short beam shear strength were found to be comparable. Dissimilar damage evolution behaviour was observed in both materials during tensile testing. The thermomechanical behaviour of the materials has been assessed as a function of temperature. Finally, fractographic investigations of shear and mode-I fracture behaviour revealed distinct fracture mechanisms that complement the findings from mechanical and thermomechanical analyses.

© 2019 The Authors. Published by Elsevier Ltd. This is an open access article under the CC BY-NC-ND license (http://creativecommons.org/licenses/by-nc-nd/4.0/).

1. Introduction

Fibre-reinforced polymer composites (FRPs) are particularly attractive for their exceptional specific strength and stiffness properties; and are known to be highly durable. Thus, they are ideal candidate materials across many sectors, particularly for weight-critical applications. They typically comprise fibrous reinforcement encapsulated within a polymer matrix, which may be thermosetting (TS) or thermoplastic (TP). TS polymers form dense three-dimensional, crosslinked networks upon polymerisation and are not thermo-softening materials; as a result, they cannot be reshaped, joined and readily recycled like their TP counterparts. Consequently, from an ecological viewpoint, TP matrices are more desirable for FRP applications; however, high melt-viscosity has been a major limitation to their cross-sectoral adoption. They typically require high-cost processing techniques where elevated

temperatures and pressures are used to realise infiltration viscosities and optimal consolidation. TS matrices possess inherently low viscosities, making them ideal for low-cost processing. In recent years, light-weighting has been identified by several sectors as an effective strategy towards meeting the strict global government targets on addressing current environmental challenges [1,2]. In the context of minimising ecological impact, TP resins possess a unique combination of characteristics that make them ideal candidate matrices for FRPs. Furthermore, TP resins have a well-documented superiority in toughness – a property that controls numerous matrix and laminate properties [3,4]. As such, the development of lower cost alternatives for TP-FRP fabrication has been the subject of extensive research.

Previous research has focussed on infusion and in-situ polymerisation of engineering polymers such as polyamide-12 (PA-12 using the laurolactam monomer system) [5], polyamide-6 (PA-6 using the caprolactam system [6,7]) and polybutylene terephthalate (PBT using cyclic oligomer precursors, known as CBT) [8–10]. In each of these cases, however, elevated mould temperatures are required in order to polymerise the matrix system after infusion into the fibre bed. Temperatures above 150 °C in the case of the PA-6 and PA-12 systems, and as high as 180 °C for the CBT are required. This can add significant expense in terms of high temperature mould tooling, especially for large structures such as wind turbine blades [11–13].

A notable advancement in this area has been the recent development of novel reactive TP resins such as Arkema's acrylic-based Elium®. These resins are low-viscosity liquids (100–200 mPa.s) at room temperature and are suited to processing by liquid composite moulding techniques using room-temperature tooling, which were once exclusively used for TS-FRP production. This technology has already been demonstrated through the production of a 9 m long glass-fibre reinforced prototype wind turbine blade using resin infusion [14]. Furthermore, the recyclability and thermoformability of these materials have also been demonstrated [15].

The properties of this infusible acrylic and its composites have been studied by many authors. These works have effectively established the knowledge base on the material's mechanical characteristics, with extensive efforts in characterising tensile, compressive, shear, impact, and fracture toughness [16–30]. Much applied research has been conducted on understanding the material's fatigue [23,31,32]; moisture diffusivity and marine ageing [33–37]; interfacial adhesion [38,39]; damage evolution and fracture behaviour [24,36,40–43]; and even the

effects of processing on properties [25,44]. Moreover, the thermomechanical properties of this acrylic family and their composites have also been studied by a number of researchers [29,40,45,46].

Several authors have published works on the comparative performance of acrylic composites with respect to comparable thermoset composites. An overview of existing literature by characterisation and reinforcement type is presented in Table 1.

Chilali et al. [24] reported comparable tensile and shear performance in both acrylic-based and epoxy-based composites. They also observed superior damage resistance in flax-acrylic composites with respect to a comparable flax-epoxy material, no differences in extent of damage and residual performance were reported between their glass-reinforced counterparts. Their findings on the tensile performance of the glass-reinforced composites are in agreement with published work by Lorriot et al. [47]; however, Baley et al. [16] reported significantly lower (−40%) tensile strength in glass-reinforced acrylic than glass-reinforced epoxy. Kinvi-Dossou et al. [28] reported superior impact performance in glass-acrylic composites than their thermoset counterparts; however, Obande et al. [29] found that despite exhibiting more energy dissipative behaviour, glass-acrylic composites were less impact damage resistant than their epoxy counterparts.

With the exception of work published by Cousins [48], the general mechanical properties (tensile, compressive, flexural and shear) of acrylic and comparable epoxy composites have not been evaluated comprehensively. As shown in Table 1, no one study comparatively evaluates general mechanical properties, fracture toughness, damage behaviour and thermomechanical characteristics in a complementary fashion. This clearly highlights the need for rigorous benchmarking to develop the robustness of the material performance database on acrylic matrices in composites, which despite attracting considerable research interest is not as well understood as traditional matrix systems such as epoxies. Such benchmarking analyses will serve to improve the understanding of areas in which acrylic composites may be most effectively applied.

In this present study, an acrylic-based glass fibre composite was benchmarked against a traditional thermosetting epoxy-based counterpart. Mechanical (tensile, flexural, short beam shear, mode-I fracture toughness) and thermomechanical characterisation techniques were used to evaluate both materials. Fractographic inspections were conducted, using scanning electron microscopy to assess shear crack modes and mode-I fracture surfaces.

Table 1
Summary of published literature on comparative performance of acrylic composites against comparable epoxy composites.

Characterisation										
Tensile	Compressive	Flexural	Shear	Fracture toughness	Impact	Fatigue	Moisture diffusivity & ageing	Damage and fracture behaviour	Damage & viscoelasticity	
F, G			F, G					F, G		Chilali et al. [24]
					G				G	Obande et al. [29]
G, C		G, C				G, C	G, C			Davies and Arhant [23]
				C						Bhudolia et al. [30]
					G					Kinvi-Dossou et al. [28]
					C					Bhudolia and Joshi [27]
			C							Bhudolia et al. [25]
			C		C					Aronica and Fossati [17]
F, J	F, J									Baley et al. [16]
							F, G			Freund et al. [35]
							G, C			Davies et al. [34]
							C			Davies [33]
							F			Chilali et al. [37]
							F	F		Chilali et al. [36]
								C	C	Bhudolia et al. [45]
G			G							Lorriot et al. [47]
G	G	G	G							Cousins [48]
G, C		G, C	G, C				G, C			Davies et al. [49]
		G								Murray et al. [50]

F, G, C and J indicate the usage of flax, glass, carbon and jute reinforcements in the cited work(s).

Table 2
Summary mechanical and thermomechanical properties reported as specified in matrix technical datasheets.

Property	Elium® 188 O	SR 1710/SD 7820
Tensile strength (MPa)	66	78
Tensile modulus (GPa)	3.2	2.8
Elongation at break (%)	2.8	6.2
Flexural strength (MPa)	111	117
Flexural modulus (GPa)	2.9	2.8
Glass transition temperature (°C)	120[a]	127

[a] Value for Elium® 280 sourced from literature [25].

2. Materials and fabrication

2.1. Materials

The materials under investigation in this study were glass fibre-reinforced acrylic (GF/acrylic) and epoxy (GF/epoxy) laminates, comprising eight plies of non-crimp E-glass fabric (TEST2594-125-50; Ahlstrom-Munksjö). Fibres in 0°- and 90°-directions and PES stitching account for 600, 36 and 10 g/m^2, respectively of the total areal weight of 646 g/m^2. For the GF/acrylic laminate, Elium® 188 O resin (Arkema) was used with BP-50-FT organic peroxide initiator (United Initiators). A two-part epoxy resin system SR 1710/SD 7820 (Sicomin Epoxy Systems), was used for the GF/epoxy laminate. The comparability of glass transition temperature (T_g) of unreinforced matrices was the main selection criterion for the reference epoxy system. It is worth noting that the mixed resin viscosities (as specified by the manufactures) were dissimilar for both resins. Elium® 188 O had a viscosity of 100 mPa.s at 25 °C, whereas the value specified for the epoxy was 450 mPa.s at 30 °C. Table 2 shows properties of both resin systems. With the exception of T_g for Elium® 188 O, all values have been sourced from relevant datasheets. Reinforcement with multi-compatible sizing was sourced for this investigation due to the limited availability of specially sized fabrics for acrylics at the time.

2.2. Manufacturing method

Laminates were manufactured using an adjustable-cavity vacuum infusion mould supplied by Composite Integration. For each processing cycle, square fabric plies measuring 485 mm in length were cut and dried in a convection oven (60 °C overnight). Eight unidirectional plies were carefully assembled into the cavity with a pre-set height of 4 mm; the entire mould surface had been pre-treated with Zyvax®

Watershield, a chemical release agent. Following the vacuum-assisted clamping and evacuation of the mould cavity, a 2-minute leak test was performed for a target maximum leak rate of 5 mbar/min. All infusions were performed at room temperature, followed by 24 h at room temperature. The GF/epoxy laminate was subjected to a two-part, free-standing post-cure (8 h at 60 °C and 4 h at 100 °C). The GF/acrylic laminate did not require post-processing; however, the recommended time of 8 h was extended to 24 h to ensure full polymerisation. As can be seen in Fig. 1, the use of the low-viscosity acrylic resin resulted in significantly shorter infusion times (up to five times shorter) than the use of its epoxy counterpart.

2.3. Preparation of test specimen

A water-lubricated diamond-coated saw blade was used to cut specimens from the fabricated laminates in accordance with relevant test standards. Drying was performed in a convection oven at 50 °C for 72 h to ensure samples were free of moisture from the cutting process prior to testing. With the exception of transverse tensile and flexural test specimens, longitudinal specimens were utilised for all other test methods.

Fibre volume and void fractions were determined by the matrix burn-off technique (ASTM D3171) to assess the quality of the laminates produced. Fibre volume fractions were the same (49.5%) in both cases; however, the void contents were 0.4% and 1.3% in GF/acrylic and GF/epoxy, respectively. The lower void content in the case of GF/acrylic can be attributed to the low infusion viscosity of the acrylic resin and is in agreement with observations by Chilali et al. [24].

3. Experimental methods

3.1. Tensile testing

Transverse tensile testing was conducted in accordance with ASTM D3039. Six samples measuring 250 mm × 25 mm were loaded at 2 mm/min until failure on an MTS Criterion (Model 45) 300-kN capacity test frame. To prevent slippage between the grip face and specimen ends during testing, 240 grit emery cloths were used at sample ends; hydraulic gripping jaws were used (grip pressure: 60 bar). Using video extensometry (Imetrum UVX & Manta G-146B/G-146C), strains were computed from recorded real-time deformations; all samples were speckled with matt black paint prior to testing.
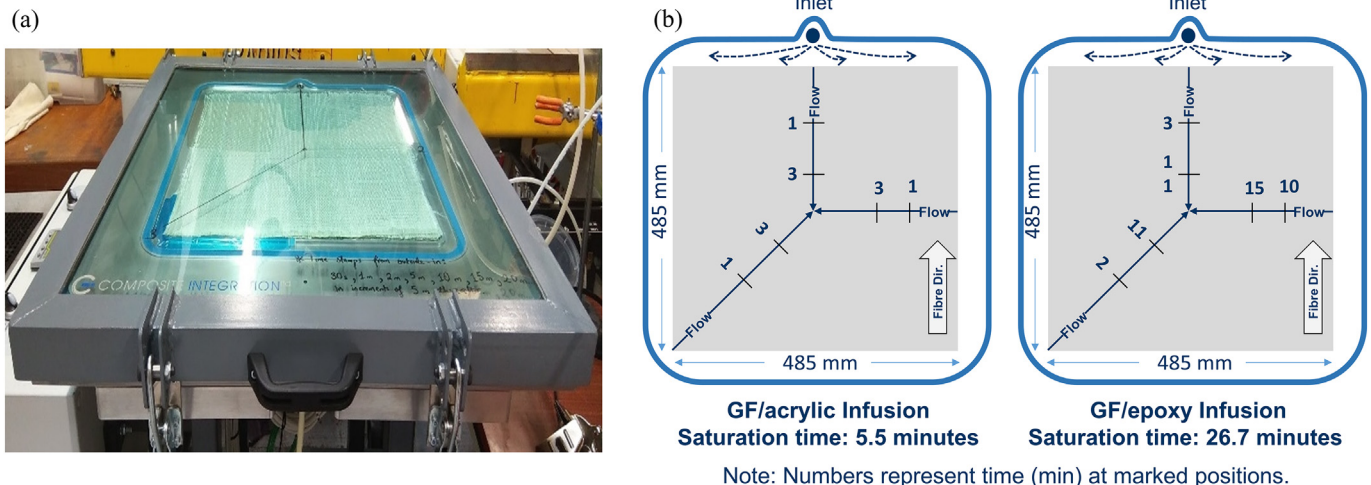

Fig. 1. (a) Experimental set-up for the production of test laminates; (b) graphical representation of observed flow fronts for GF/acrylic and GF/epoxy.

Analyser	Q800-V21.1 TA instruments
Mode	Three-point bending (longitudinal)
Nominal specimen dimensions	60 mm × 10 mm × 4 mm (50-mm span)
Temperature profile	Ambient – 180 °C (3 °C/min)
Displacement amplitude	50 μm
Frequency	1 Hz

3.2. Flexural testing

The longitudinal and transverse flexural properties (strengths and moduli) of GF/acrylic and GF/epoxy were determined by three-point loading in accordance with ASTM D7264 using a sample span-to-thickness ratio of 32:1, corresponding to sample lengths of 154 mm and crosshead speed of 1 mm/min. Loading nose and supports were hardened steel pins of 6 mm diameter. Six samples were tested for each material under transverse loading conditions, whereas five samples were loaded longitudinally from each laminate. Testing was performed on an Instron (3369) test frame fitted with a 10 kN load cell (Instron 2530-10 kN). Mid-span deflections were tracked and recorded by means of the video extensometer described in Section 3.1. Sample edges were speckled with a fine-tip permanent marker to facilitate video extensometry.

3.3. Short beam shear testing

To evaluate the short beam shear performance of GF/acrylic and GF/epoxy, six coupons measuring 8 mm × 24 mm were loaded to failure by short beam shear testing (in accordance with ASTM D2344). The test frame detailed in Section 3.2 was used. Testing was performed at a crosshead speed of 1 mm/min. A span-to-thickness ratio of 4:1 was used to ensure samples were subjected to a shear stress state. Cylindrical loading nose and supports were used with diameters of 6 mm and 3 mm, respectively.

3.4. Mode-I fracture toughness testing

Double cantilever beam (DCB) testing was performed in accordance with ASTM D5528 for the determination of mode-I interlaminar fracture toughness. Testing was performed on the Instron test frame detailed in Section 3.2. Self-releasing films (13-μm thick perfluoroalkoxy alkane) were implanted at the mid-plane of each laminate during fabrication to create a 63-mm long initiation site for delamination. Samples were carefully cut from the test laminate to maintain the length of the original initiation site and dimensions (175 mm × 25 mm). Steel loading blocks (25 mm × 25 mm × 16 mm) were bonded to the *pre-cracked* sample ends for load introduction and high-contrast speckles were applied as described in Section 3.2 to sample edges to facilitate automatic tracking of delamination length using a video extensometer (refer to Section 3.1

for specifications). For each test, loading was performed at a rate of 1 mm/min for a minimum delamination length of 50 mm. Load, opening (crosshead) displacement and delamination length were recorded.

3.5. Dynamic mechanical analysis

Dynamical mechanical analysis (DMA) was performed in accordance with BS ISO 6721-11 to assess the thermomechanical properties of both materials. The test and specimen specifications are detailed in Table 3. Storage and loss moduli, and tan delta were recorded as functions of temperature throughout testing.

3.6. Scanning electron microscopy

Scanning electron microscopy was used as a means of qualitatively assessing failure behaviour following short beam shear (SBS) and DCB testing. Samples were prepared with a 40-nm sputter coating of gold to enhance surface conductivity and imaged at 5 kV on a JEOL JSM series instrument. SBS sample edges were coated; whereas on DCB samples, coating was applied to exposed interlaminar fracture surfaces (created during testing).

4. Results and discussion of manufactured laminates

4.1. Results of mechanical characterisation

A summary of the tensile, flexural and short beam shear properties reported and discussed in Sections 4.1.1 to 4.1.4 is presented in Table 4.

4.1.1. Transverse tensile test results
Representative stress-strain responses for GF/acrylic and GF/epoxy are presented in Fig. 2 and are given in Table 4. GF/acrylic exhibited significantly higher average transverse tensile strengths at 73 MPa, compared to 54 MPa for the GF/epoxy specimens. For both materials, strain is observed to increase linearly with increasing applied stress. GF/acrylic samples showed evidence of plastic deformation at strains in excess of 0.4% and continue to yield gradually until the point of ultimate specimen fracture. In contrast, lower transverse tensile strengths were observed for the GF/epoxy samples, with higher strains observed at failure. GF/epoxy had higher failure strains (2.1 ± 0.2%) than GF/acrylic (1.2 ± 0.3%).

As shown in Fig. 3, a series of horizontal cracks were observed in all GF/epoxy specimens. In the case of GF/acrylic, only a few cracks were seen to appear prior to the main failure event. Evidence of fibre-splitting along the loading direction, originating from the sparsely distributed 90°-fibres were only observed in GF/acrylic samples.
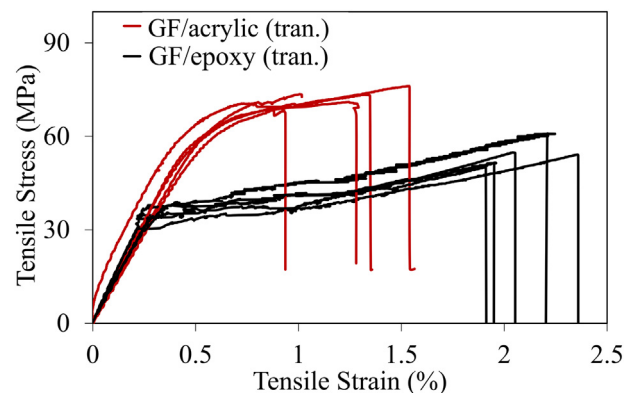
Table 4
Tensile, flexural and shear properties.

		GF/acrylic	GF/epoxy
Tensile properties (transverse)	Strength (MPa)	73 ± 3.9	54 ± 4.1
	Modulus (GPa)	13 ± 0.6	13 ± 0.5
	Failure strain (%)	1.2 ± 0.3	2.1 ± 0.2
Flexural properties (longitudinal)	Strength (MPa)	879 ± 49	869 ± 42
	Modulus (GPa)	40 ± 1.7	38 ± 2.3
	Failure strain (%)	3.3 ± 0.4	3.4 ± 0.6
Flexural properties (transverse)	Strength (MPa)	91 ± 5.4	94 ± 7.2
	Modulus (GPa)	11 ± 0.2	12 ± 0.4
	Failure strain (%)	1.7 ± 0.3	2.0 ± 0.2
Short beam shear properties	Strength (MPa)	58 ± 1.7	57 ± 1.0

Fig. 2. Transverse stress-strain behaviour of all GF/acrylic and GF/epoxy samples. Reinforcements are a non-crimp stitched unidirectional E-glass fabric with fibre volume fraction of 49.5% in each case.
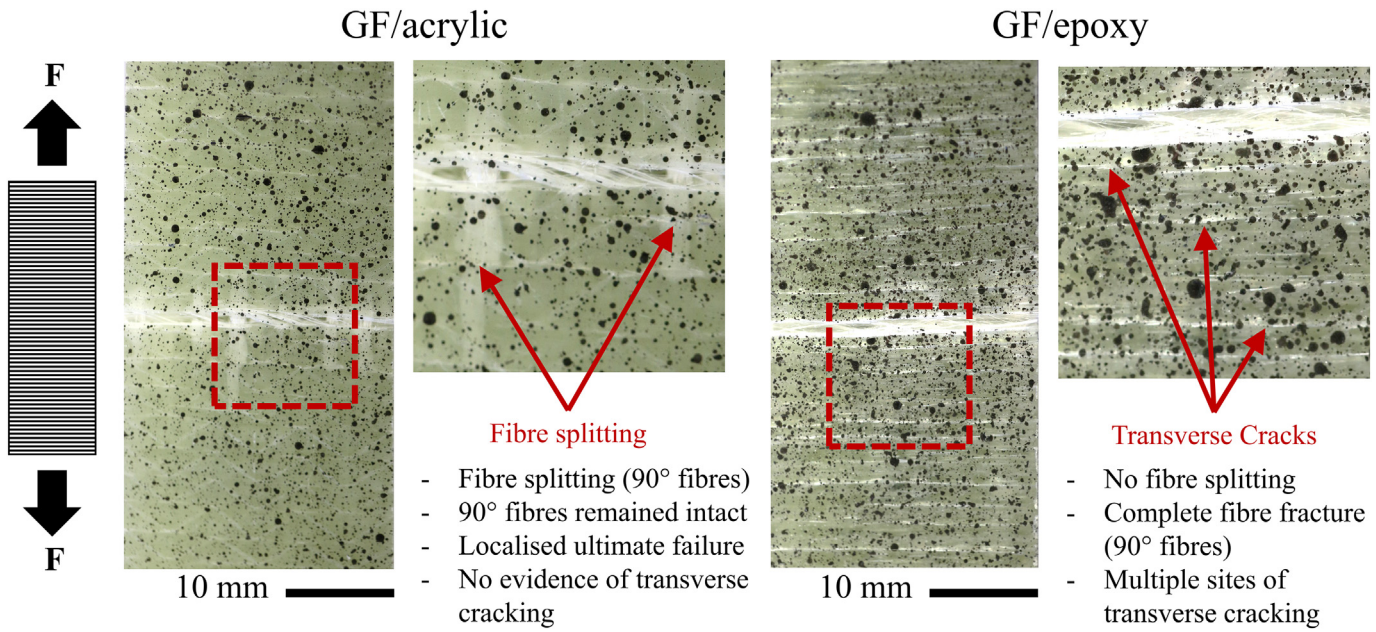
GF/acrylic

GF/epoxy

- Fibre splitting (90° fibres)
- 90° fibres remained intact
- Localised ultimate failure
- No evidence of transverse cracking

- No fibre splitting
- Complete fibre fracture (90° fibres)
- Multiple sites of transverse cracking

Fig. 3. Representative failure modes in both materials following transverse tensile testing with loading direction schematically represented.

Strain maps (obtained from video extensometer) have been presented in time-lapse sequences (Fig. 4) to highlight the difference in strain development (and thus, damage evolution) between both material systems. GF/acrylic strain maps are more uniform throughout the testing. The effects of accumulating transverse cracks in GF/epoxy, however, are highly evident; high-strain domains dominate the strain maps between 40 min and t*. The time stamp, t* represents the strain distribution at the time of ultimate failure in both materials.
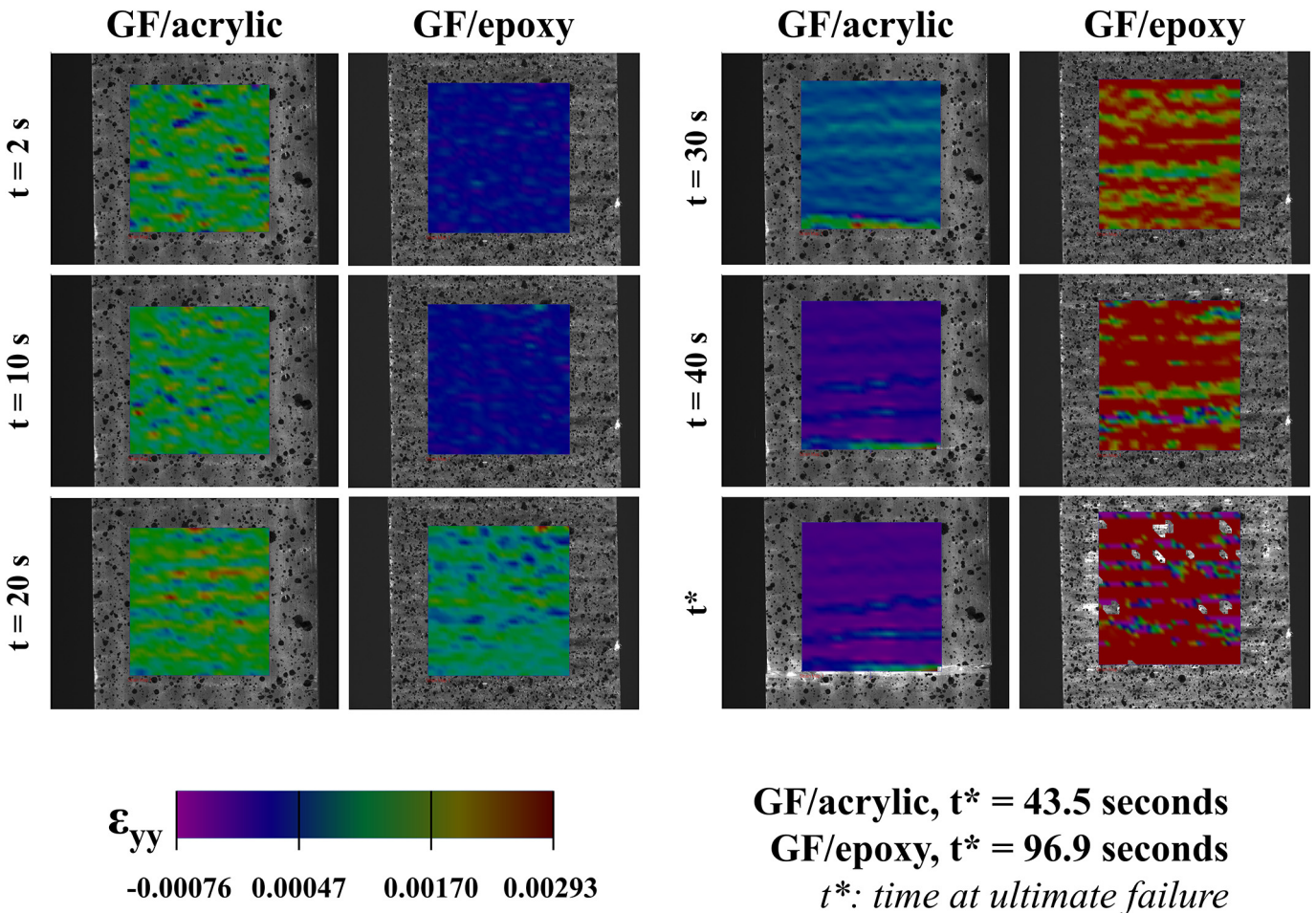

GF/acrylic, t* = 43.5 seconds
GF/epoxy, t* = 96.9 seconds
t: time at ultimate failure*

Fig. 4. Time-lapse compilation of representative strain maps obtained during transverse tensile loading of GF/acrylic and GF/epoxy samples.

4.1.2. Longitudinal flexural test result

Fig. 5 shows representative stress-strain behaviour of the materials under investigation following longitudinal flexural loading to failure. As previously presented in Table 4, GF/acrylic exhibited marginally higher strength (average of 880 MPa) and modulus (average of 40 GPa) compared to averages of 870 MPa and 38 GPa for GF/epoxy, respectively. In addition, up to failure, its stress-strain response was similar to that of GF/epoxy.

A monotonic linear increase in stress exists in both materials up to the limit of proportionality; thereafter, evidence of plastic deformation is seen until the onset of severe compressive failure (Point 1). However, they exhibit dissimilar damage evolution beyond this point. In both materials, ultimate tensile fibre fracture (Point 2) is observed as a discrete and sudden loss in stiffness; however, in GF/acrylic samples, this was preceded by an extended period where marginal stress reductions were observed with increasing strain. This behaviour is thought to be indicative of progressive matrix cracking [51]. In the case of the GF/epoxy samples, more sudden load drops and stepped reduction in stress are observed until ultimate failure. The strain window between onset and ultimate failure events, i.e., between Points 1 and 2 was broader (~26%) in GF/acrylic samples.

Damage initiation in both materials occurred on the side in compression, with evidence of compressive fibre fractures being observed before tensile fibre fracture. In the case of GF/epoxy samples, tensile matrix failure events coincided with compressive fibre fracture. It is worth noting however, that as these observations were reliant on edge detection of failure, other undetected failure events may have occurred prior to those reported.

Post-mortem inspections of ultimate compressive, tensile and through-thickness (edge) failure modes were conducted on all samples. Representative images obtained during these inspections are presented in Fig. 6. Focusing on the damage on the compressive sides (Fig. 6a & d) of test samples from both materials, distinct failure types are observed; GF/acrylic samples showed evidence of micro-buckling under the loading nose and severe delamination in tows on outer edges. On the other hand, matrix crushing was more prominent in GF/epoxy, without edge effect as observed with GF/acrylic. A lesser extent of surface buckling was evident. Distinct, ultimate tensile failure modes were also observed in both materials. While all samples showed characteristics of tow separation and delamination, GF/acrylic tows remained mostly intact (Fig. 6b), whereas GF/epoxy tows suffered more intra-tow matrix cracks and debonding, leading to a shinier appearance (Fig. 6e). Damage in GF/acrylic was spread over a longer length, while more localised damage occurred in GF/epoxy. Comparing the distribution of damage mechanisms through the thickness as shown in Fig. 6c and f, a similar extent of fibre-related damage processes (such as kinking and fracture) were observed in both materials. Although distinct regions of compressive and tensile failure were observed in all samples, GF/acrylic samples showed more *hourglass-shaped* distribution of these regions, with upper and lower regions joining. In contrast, GF/epoxy samples had two discrete upper and lower bounds in the distribution of failure.

4.1.3. Transverse flexural test results

Representative stress-strain responses to transverse flexural loading are shown in Fig. 7. and strengths and moduli were presented in Table 4.
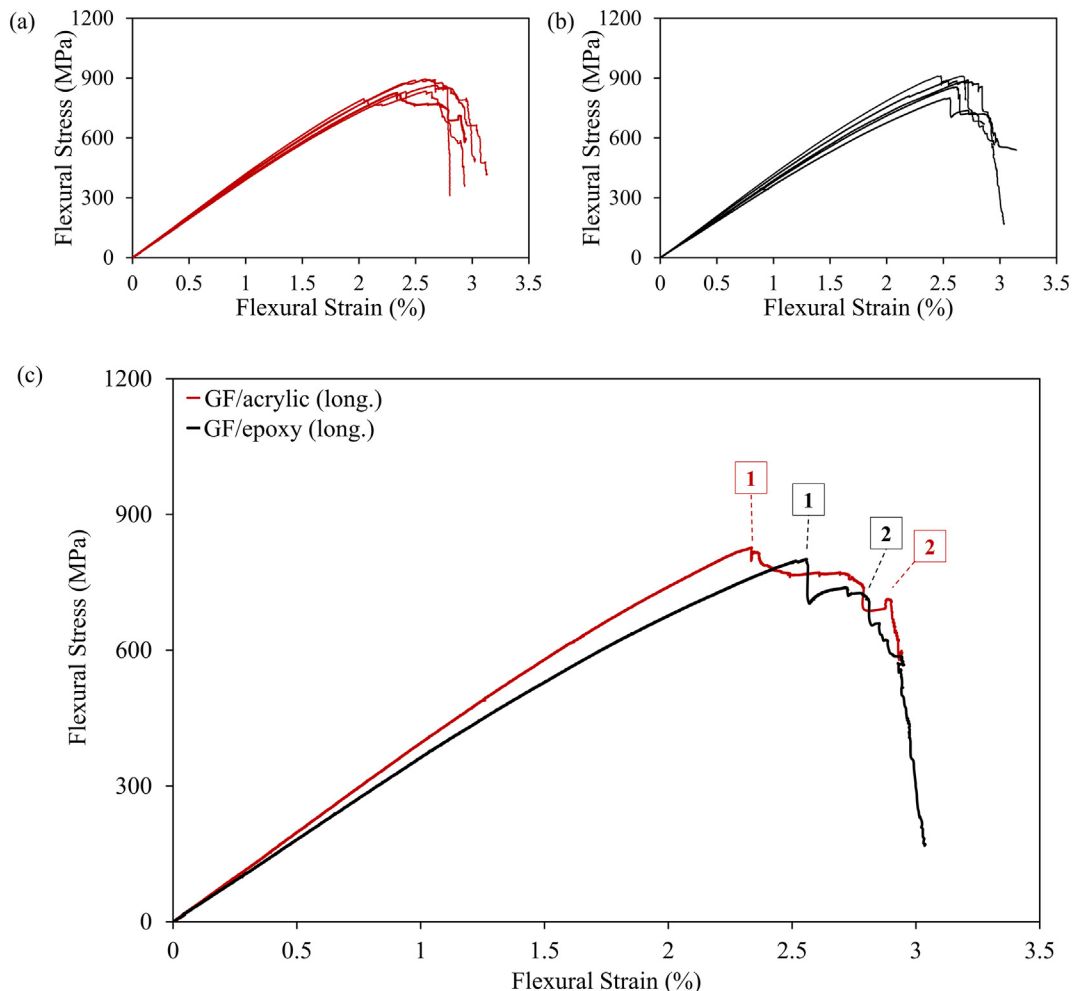

Fig. 5. Stress-strain curves of (a) GF/acrylic, (b) GF/epoxy and (c) representative curves showing characteristic behaviour of both materials in response to longitudinal flexural loading.
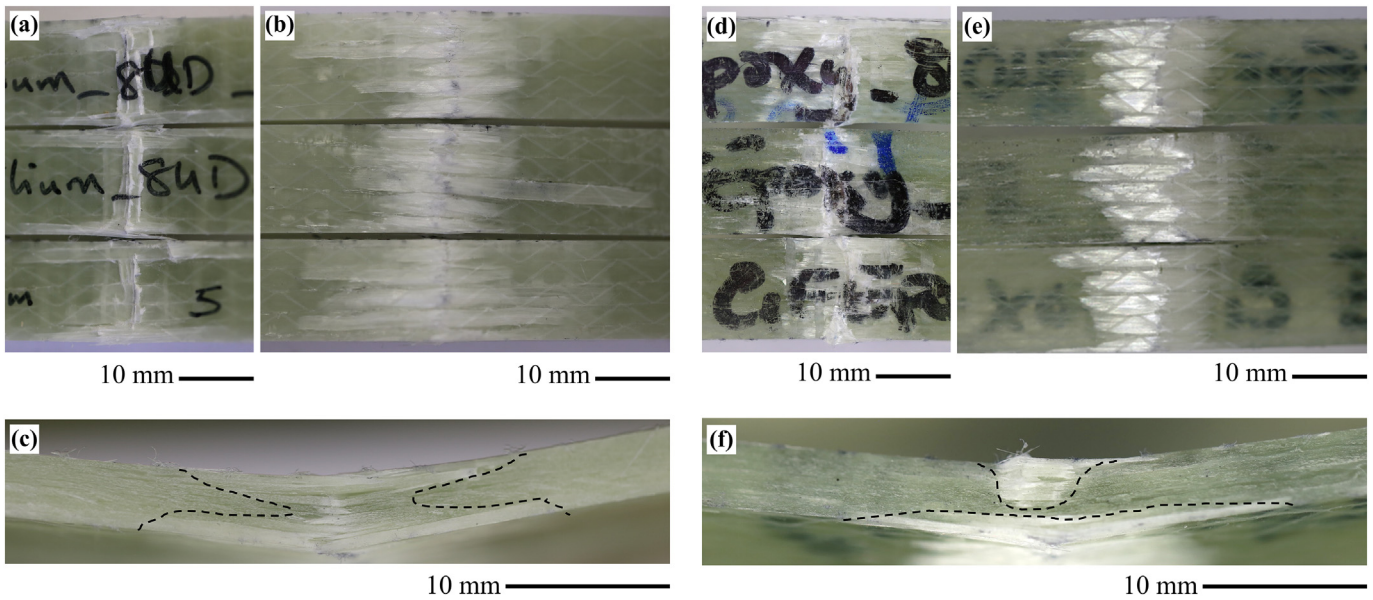
Fig. 6. Images showing representative modes of (a) compressive failure, (b) tensile failure, on upper and lower surfaces, respectively; and (c) regions of compressive and tensile failure on GF/acrylic sample edges of longitudinal flexure specimens. Note: (d), (e) and (f) are same features on GF/epoxy samples, respectively.
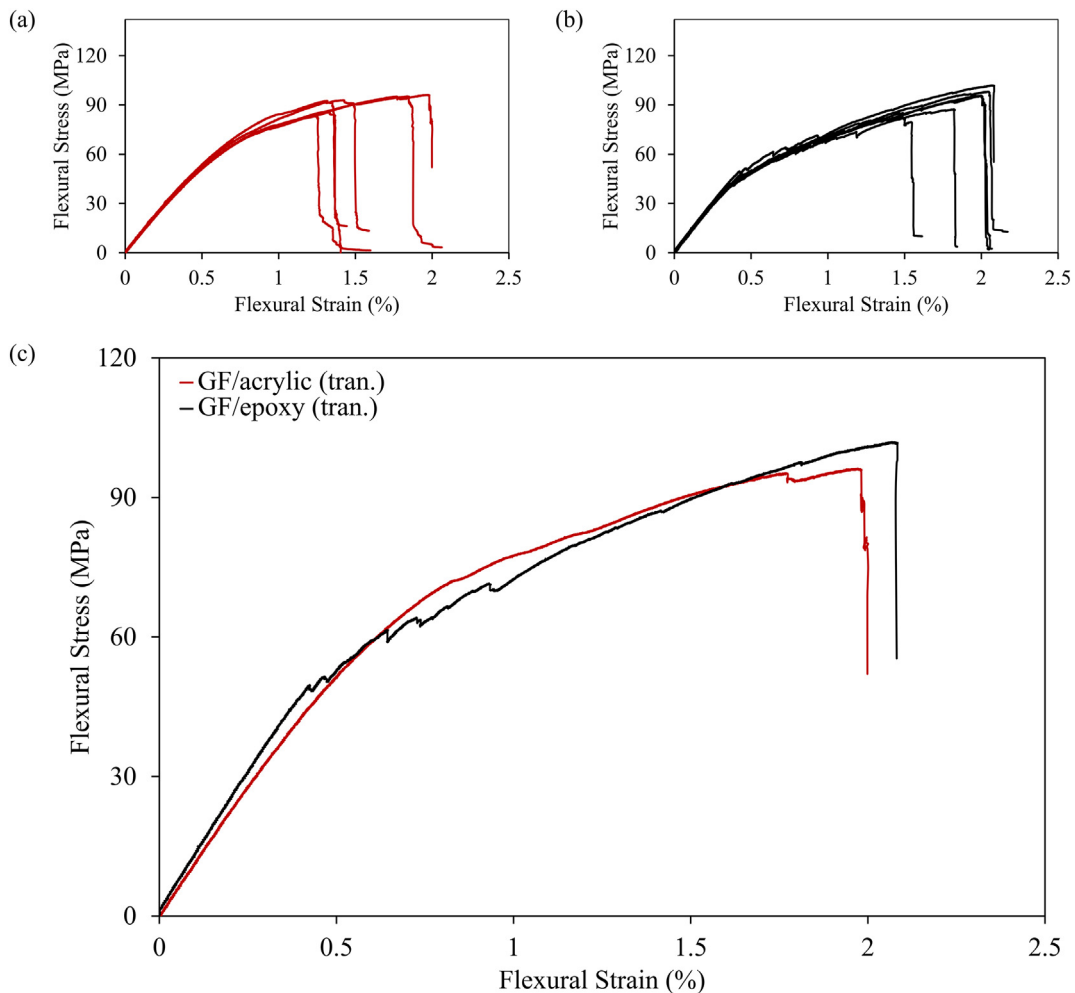

Fig. 7. Stress-strain curves of (a) GF/acrylic and (b) GF/epoxy and (c) representative curves showing characteristic behaviour of both materials in response to transverse flexural loading.
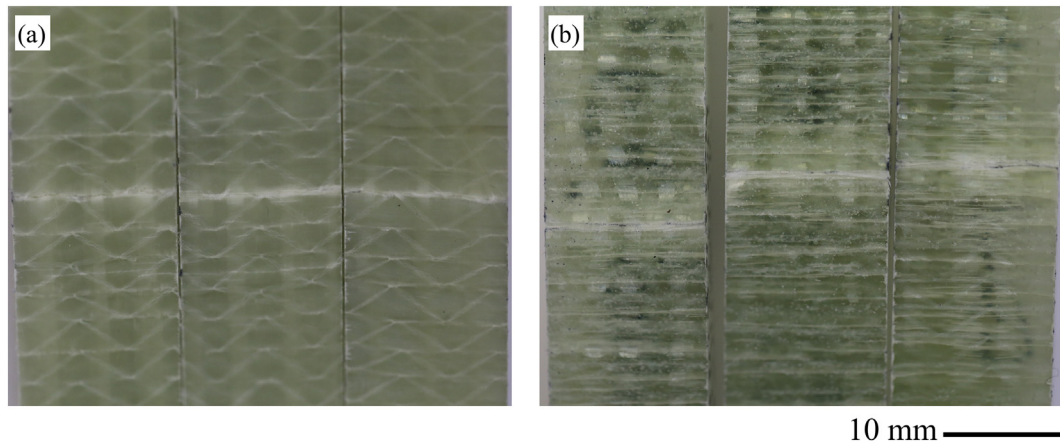
Fig. 8. Images of representative failures (tensile side) on three samples of (a) GF/acrylic and (b) GF/epoxy following transverse flexural testing.

Despite its superior transverse tensile performance, with strength of 91 MPa and modulus of 11 GPa, GF/acrylic had marginally lower transverse flexural properties than GF/epoxy, which had average strength of 94 MPa and modulus of 12 GPa.

As seen in Fig. 7, both materials exhibit a short linear elastic region, however, in the case of GF/acrylic; this region is followed by some nonlinearity until failure, indicating a higher degree of plastic deformation before failure. Conversely, GF/epoxy samples showed evidence of earlier onset of damage after the initial linear region. In all epoxy-based samples, this region was followed by oscillations in stress-strain response (indicating progressive accumulation of minor damage events) until the occurrence of ultimate failure. Unlike the longitudinal stress-strain responses where a broader region of linearity was observed (indicating fibre-dominated flexural behaviour), a high extent of non-linearity
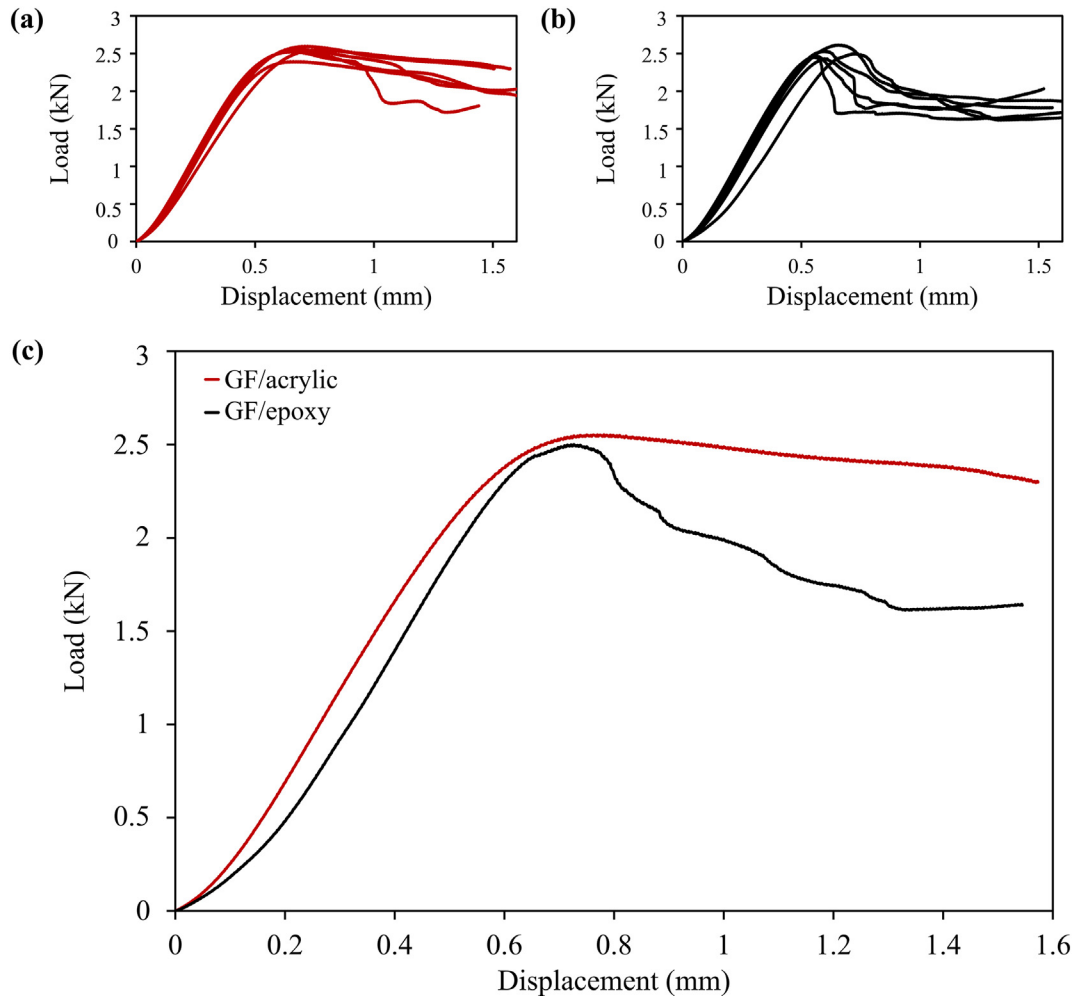

Fig. 9. Load-displacement curves obtained from short beam shear tests for all (a) GF/acrylic and (b) GF/epoxy samples and (c) a comparison of two representative curves from both materials.

exists in the transverse stress-strain curves due to the matrix-dominated nature of failure.

As shown in Fig. 8, multiple transverse cracks were observed on GF/Epoxy samples, explaining the oscillations observed in stress-strain behaviour (Fig. 7) leading to ultimate failure. In GF/acrylic, fewer cracks were evident; however, these were concentrated around the main site of matrix fracture.

4.1.4. Short beam shear test results

In this section, the results of short beam shear testing for the determination of short shear strengths are presented in Table 4 and discussed. GF/acrylic had marginally higher average shear strength (58 MPa) than GF/epoxy (57 MPa). Fig. 9 shows all load-displacement curves for both materials.

Load-displacement curves reveal similar pre-peak behaviour in both materials. A linear region is observed for all samples and is followed by some nonlinear deformation prior to peak load. Beyond this point, GF/acrylic samples did not exhibit abrupt load drops; their curves revealed evidence of severe inelastic deformation with localised stable crack propagation. In contrast, a more noticeable onset of failure is observed in GF/epoxy samples as load drops of about 20–30% from respective load peaks. Larger areas are bounded by the GF/acrylic curves than those observed under GF/epoxy curves, indicating higher energy absorption. It can thus be assumed that more fracture energy was available within GF/acrylic samples.

Post-mortem SEM inspections on edges of failed specimens were conducted to substantiate observed load-displacement behaviour. As shown in Fig. 10, evidence of interlaminar shear and plastic deformation are visible in GF/acrylic, with ductile fracture characteristics observed. The damage characteristics of GF/epoxy shown in Fig. 11 are consistent

with interlaminar shear failure; brittle shear cusps [52] were present, with no plasticity being observed. Both materials had multiple cracks uniformly dispersed throughout the thickness.

All cracks observed in the GF/epoxy sample were near 90° fibres, which were dispersed throughout each ply. In contrast, cracks in GF/acrylic did not occur around these fibres. The observation of more delamination in GF/acrylic than GF/epoxy are in agreement with the assumptions made from the load-displacement curves in terms of fracture energy absorption.

4.1.5. Interlaminar fracture toughness

It has been shown in preceding sections that GF/acrylic significantly outperforms GF/epoxy in terms of transverse tensile strength, while exhibiting similar interlaminar short beam shear and flexural properties (in both longitudinal and transverse directions). This section discusses the observations from double cantilever beam fracture testing. The mode-I fracture toughness values reported here are average strain energies released during initiation ($G_{IC-Init.}$) and propagation ($G_{IC-Prop.}$), calculated using the modified beam theory method as per the test standard, with the onset of nonlinearity being used to evaluate the former.

GF/acrylic exhibited superior mode-I fracture toughness, with a mean $G_{IC-Prop.}$ of 1814 J/m^2 compared to the value of 1574 J/m^2 for GF/epoxy, with 19% higher initiation fracture toughness than GF/epoxy. Representative load-displacement curves, R-curves and comparison of mean initiation and propagation toughness values are presented in Fig. 12.

All samples exhibited an initial non-linearity during the *take-up* portion of load introduction and simultaneous opening of the specimen prior to crack initiation. Following this, a monotonic increase in load
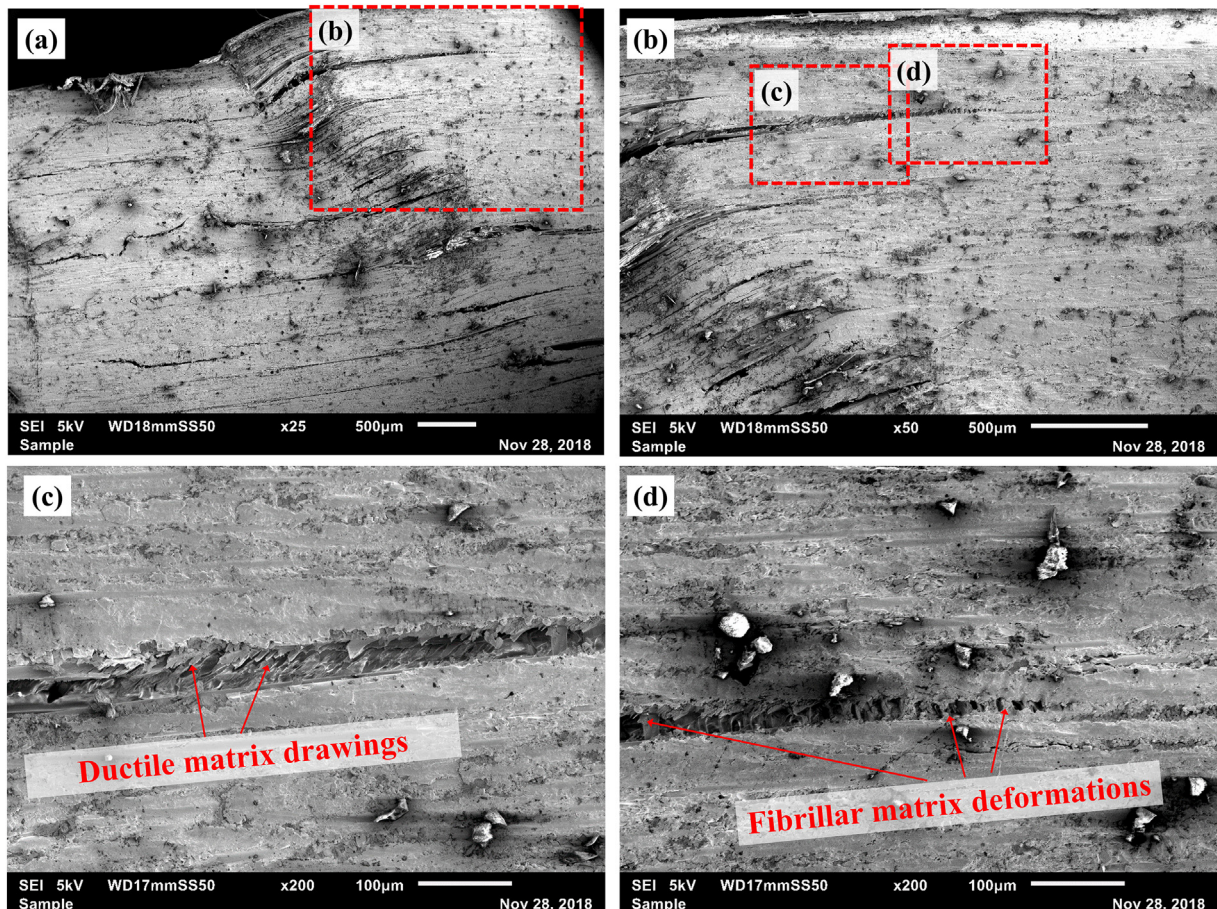

Fig. 10. SEM micrographs showing representative GF/acrylic short beam shear failure modes at magnifications of 25× in (a), 50× in (b), and 200× in (c) and (d).
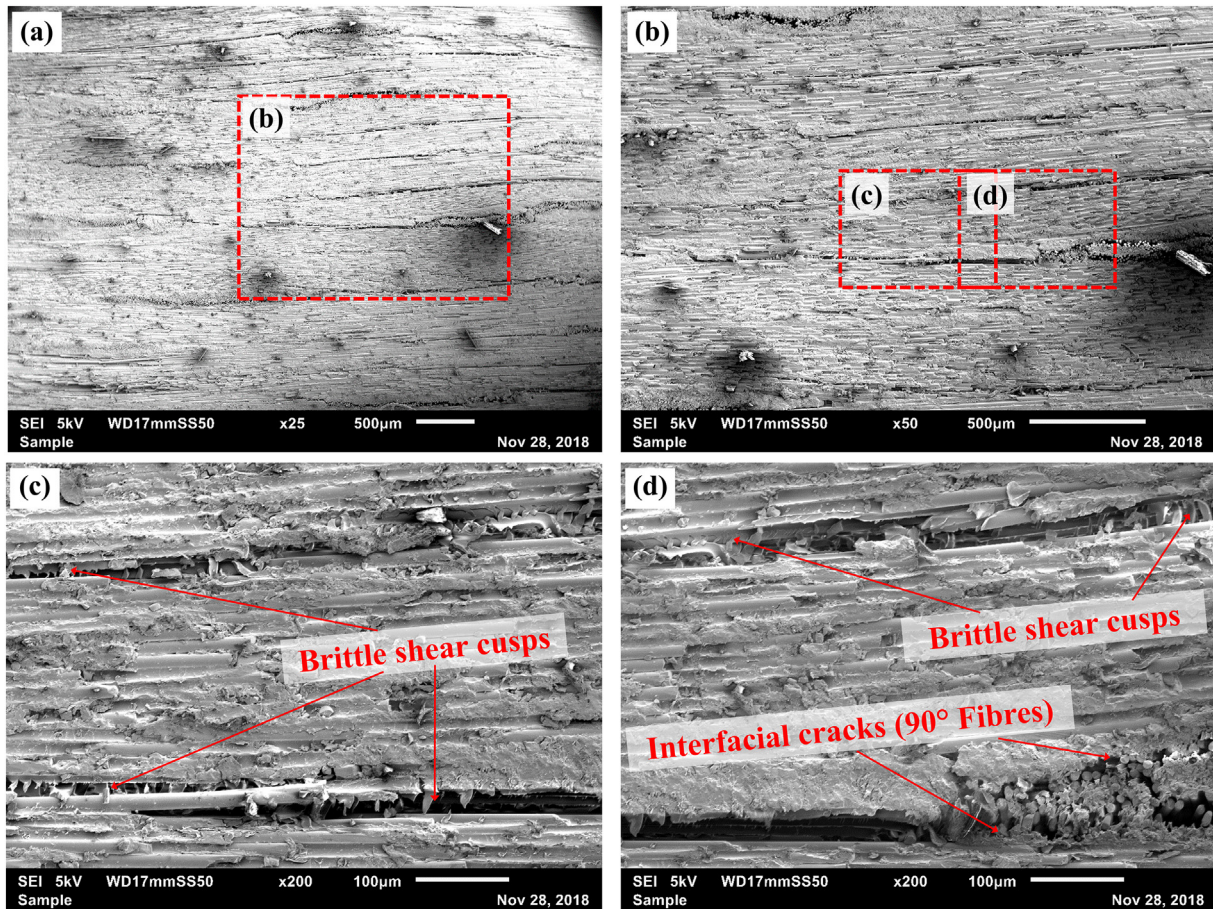
Fig. 11. SEM micrographs showing representative GF/epoxy short beam shear failure modes at magnifications of 25× in (a), 50× in (b), and 200× in (c) and (d).

was observed prior to delamination initiation. A minor pre-peak load-drop is evident in both materials. Upon initiation, the load-displacement curves of both materials showed minor oscillations and load-drops, which are consistent with stick-slip delamination behaviour (indicative of unstable propagation) [53,54].

From Fig. 13, a higher extent of fibre bridging (at the crack tip) is observed in GF/acrylic than in GF/epoxy. Moreover, crack bridging occurred throughout testing due to the presence of 90° tows in the fabric used. This was evident in both materials and occurred throughout testing; as such, the load-displacement curves (Fig. 12a) and the R-curves (Fig. 12b) are not representative of purely unidirectional

specimens. It is highly likely that some of the load drops and evolution of mode-I fracture resistance with increasing crack length correspond to secondary energy-dissipation processes such as tow rupture and/or debonding events [54]. However, as the same reinforcement was used in both materials, the associated effects on the comparability of these materials are considered negligible. As is evident in Fig. 12b, the delamination resistance of GF/acrylic increases with increasing crack growth, whereas that of GF/epoxy remains relatively constant.

Focusing on electron micrographic inspections of fracture surfaces (Fig. 14) however, distinct failure modes are visible in both materials. The presence of ductile matrix deformation and risers on the GF/acrylic
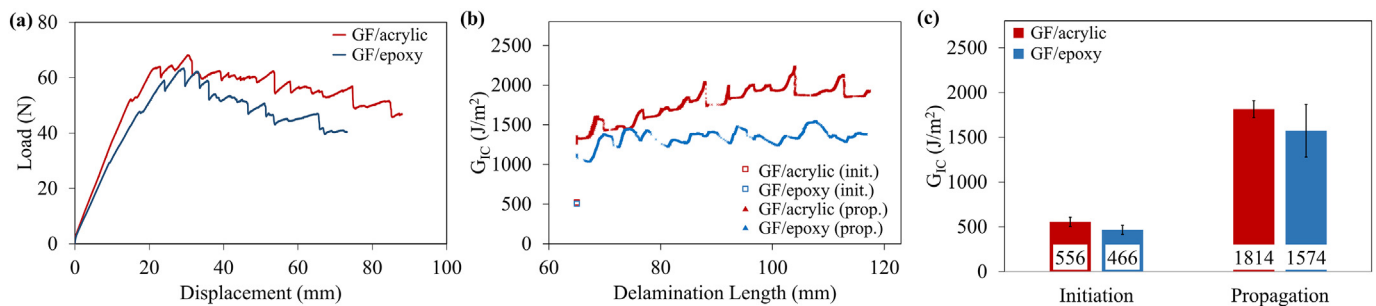

Fig. 12. Representative (a) load-displacement curves and (b) resistance curves (R-curves) obtained from DCB testing of GF/acrylic and GF/epoxy; and (c) is a chart comparing their average $G_{IC\text{-Init.}}$ and $G_{IC\text{-Prop.}}$ values.
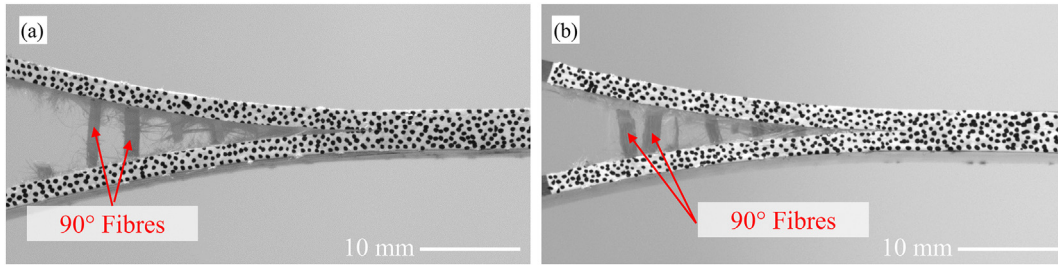
Fig. 13. Images of representative delamination behaviour observed during DCB testing of (a) GF/acrylic and (b) GF/epoxy at equivalent test times.
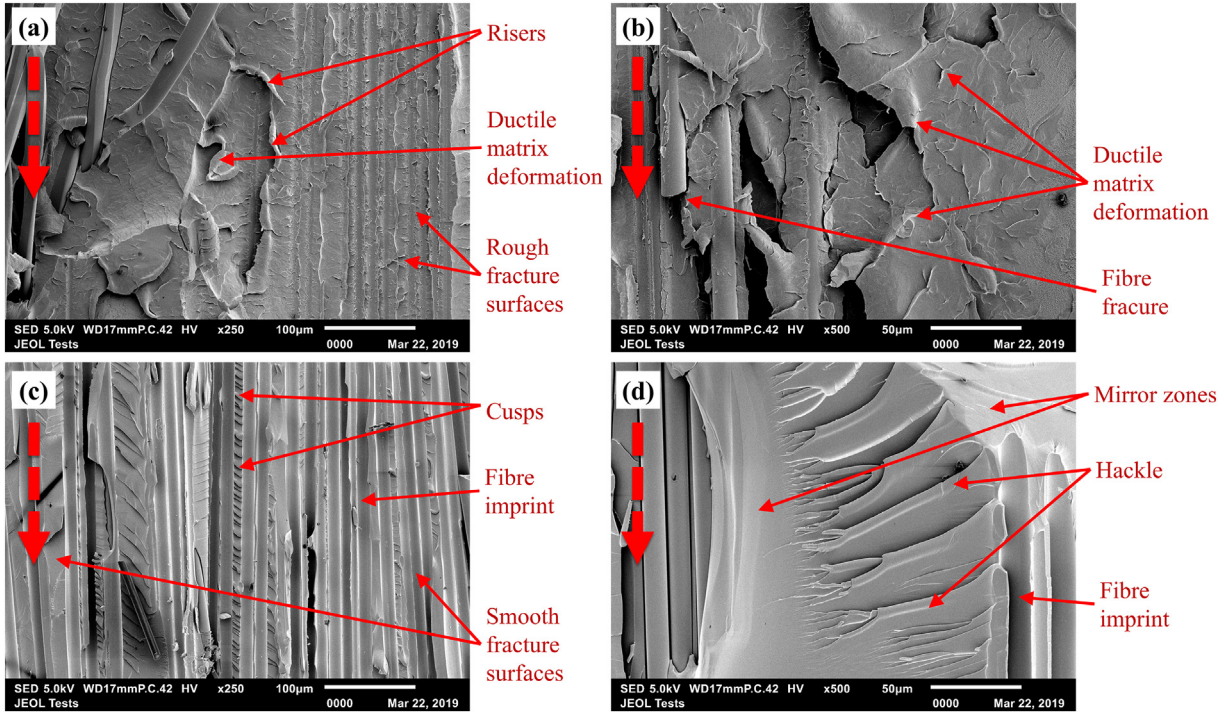

Fig. 14. SEM micrographs of mode-I fracture surfaces of GF/acrylic (a–b) and GF/epoxy (c–d).

fracture surface indicated ductile matrix fracture, whereas the cusps, mirror zones and hackle zones observed in GF/epoxy are characteristics of brittle matrix fracture. In the context of ductile and brittle matrix fracture characteristics, these micrographic observations are consistent with those from short beam test specimens. Moreover, an exceptional level of fibre-matrix adhesion was observed in GF/acrylic compared with its epoxy counterpart. This explains the superiority in transverse tensile strength in the GF/acrylic material and confirms that the use of fabric with multi-compatible sizing resulted in a desirable strong interfacial adhesion. In addition to the presence of risers, matrix fractures observed in GF/acrylic were distinctly duller in appearance and seemed to have a rougher texture, further confirming microscopic ductile fracture. All epoxy matrix fractures had brittle characteristics (sheen and smoothness).

4.2. Dynamic mechanical analysis

The viscoelastic response of both materials with temperature are shown in Fig. 15. The section that follows discusses differences in tan delta and storage modulus for both materials in the context of damping behaviour associated with each matrix type.

The thermomechanical properties of GF/acrylic and GF/epoxy obtained from the DMA experiments are presented in Table 5.

GF/acrylic was found to exhibit superior damping behaviour, as evidenced by the higher tan delta peak and the larger area under this peak, compared to GF/epoxy. The term "damping" here is used to indicate the energy dissipative efficiency of the materials [55,56]. The area bounded
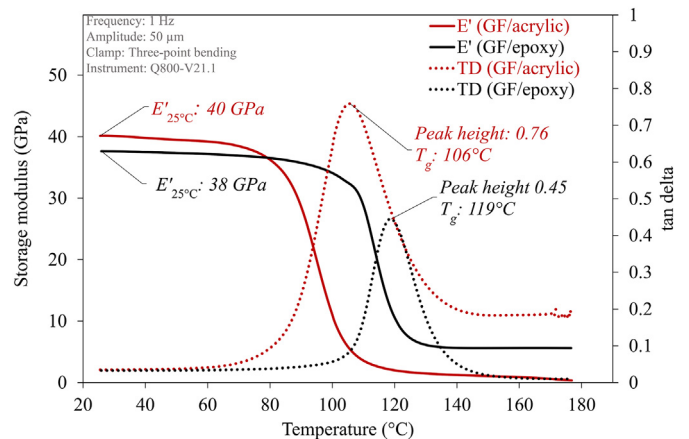

Fig. 15. Thermomechanical results showing the effect of temperature on storage modulus and tan delta in DMA testing. Testing carried out in the longitudinal direction.

Table 5
Summary of thermomechanical results.

	T_g, tan delta (°C)	Height of tan delta peak	Storage modulus at onset (GPa)
GF/acrylic	106	0.76	40
GF/epoxy	119	0.45	38

under the tan delta curve is proportional to the degree of molecular mobility, which in turn correlates to damping properties [57,58]. Thus, having higher peak intensity and larger area under its tan delta curve, GF/acrylic exhibits better damping behaviour. Being a thermoplastic amorphous polymer, i.e., possessing no crosslinks, the polymer chains in GF/acrylic can undergo instantaneous short-range deformation to dissipate the applied stresses. Conversely, the crosslinked 3D-network structure of the matrix in GF/epoxy inhibits deformations of the same magnitude as observed in GF/acrylic. The effects of crosslinks on the height of tan delta peaks have been previously studied by Bandzierz et al. [59]. These results indicate that GF/acrylic would tend towards highly inelastic response, whereas elastic response dominates in GF/epoxy.

5. Conclusions

The present research comparatively assessed the mechanical and thermomechanical performance of a vacuum-infused thermoplastic acrylic composite against a traditional epoxy based system. The processing of the thermoplastic system was associated with shorter cycle times (due to low viscosity infiltration and no requirement for post-processing). Moreover, the use of multi-sized reinforcement fabric resulted in good interfacial adhesion in GF/acrylic.

The following are the relevant findings and observations in relation to the benchmarking of GF/acrylic against GF/epoxy:

- GF/acrylic had 33% higher transverse tensile strength and equivalent modulus.
- It had comparable longitudinal flexural strength (+1%) and modulus (+5%).
- Its short beam shear strength was comparable (+2%).
- It had slightly lower transverse flexural strength (−3%) and modulus (−8%).
- It exhibited superior fracture toughness and delamination resistance with its $G_{IC-Init.}$ and $G_{IC-Prop.}$ being 19% and 15% higher, respectively.
- Micrographs revealed microstructural ductility in GF/acrylic and brittle fracture mechanisms in GF/epoxy.
- GF/acrylic had a higher tan delta peak (+69%) than GF/epoxy.

The findings and observations presented in this paper will serve to foster an understanding of acrylic matrices in continuous fibre-reinforced composite applications. Such knowledge is essential for highlighting applications where acrylic-based composite may most effectively be employed, and may provide guidance on necessary performance enhancing modifications.

CRediT authorship contribution statement

Winifred Obande: Conceptualization, Data curation, Formal analysis, Investigation, Methodology, Project administration, Resources, Visualization, Writing - original draft, Writing - review & editing. **Dimitrios Mamalis:** Data curation, Formal analysis, Investigation, Writing - review & editing. **Dipa Ray:** Conceptualization, Funding acquisition, Methodology, Project administration, Resources, Supervision, Validation, Visualization, Writing - review & editing. **Liu Yang:** Formal analysis, Resources, Validation. **Conchúr M. Ó Brádaigh:** Funding acquisition, Resources, Supervision, Validation, Writing - review & editing.

Declaration of conflicting interests

The authors declared no potential conflicts of interest with respect to the research, authorship, and/or publication of this article.

The raw/processed data required to reproduce these findings cannot be shared at this time due to technical or time limitations.

References

[1] H.J. Kim, G.A. Keoleian, S.J. Skerlos, Economic assessment of greenhouse gas emissions reduction by vehicle lightweighting using aluminum and high-strength steel, J. Ind. Ecol. 15 (2011) 64–80, https://doi.org/10.1111/j.1530-9290.2010.00288.x.

[2] H. Helms, U. Lambrecht, The potential contribution of light-weighting to reduce transport energy consumption, Int. J. Life Cycle Assess. 12 (2006) 58–64, https://doi.org/10.1065/lca2006.07.258.

[3] N.H. Nash, T.M. Young, P.T. McGrail, W.F. Stanley, Inclusion of a thermoplastic phase to improve impact and post-impact performances of carbon fibre reinforced thermosetting composites - a review, Mater. Des. 85 (2015) 582–597, https://doi.org/10.1016/j.matdes.2015.07.001.

[4] K.-Y. Kim, L. Ye, K.-M. Phoa, Interlaminar fracture toughness of CF/PEI and GF/PEI composites at elevated temperatures, Appl. Compos. Mater. 11 (2004) 173–190 https://link.springer.com/content/pdf/10.1023%2FB%3AACMA.0000026586.12629.7e.pdf (accessed December 7, 2018).

[5] P. Ó Máirtín, P. McDonnell, M. Connor, R. Eder, C.M. Ó Brádaigh, Process investigation of a liquid PA-12/carbon fibre moulding system, Compos. Part A 32 (2001) 915–923www.elsevier.com/locate/compositesa, Accessed date: 29 December 2018.

[6] K. Van Rijswijk, J.J.E. Teuwen, H.E.N. Bersee, A. Beukers, Textile fiber-reinforced anionic polyamide-6 composites. Part I: the vacuum infusion process, Compos. Part A Appl. Sci. Manuf. 40 (2008) 1–10, https://doi.org/10.1016/j.compositesa.2008.03.018.

[7] S. Pillay, U.K. Vaidya, G.M. Janowski, Effects of moisture and UV exposure on liquid molded carbon fabric reinforced nylon 6 composite laminates, Compos. Sci. Technol. 69 (2009) 839–846, https://doi.org/10.1016/j.compscitech.2008.03.021.

[8] S.M. Coll, A.M. Murtagh, C.M. Ó Brádaigh, Resin film infusion of cyclic pBT composites: a fundamental study, in: Proc. SAMPE Eur. 25th Int. Jubil. Conf., Paris, 2004.

[9] H. Parton, I. Verpoest, In situ polymerization of thermoplastic composites based on cyclic oligomers, Polym. Compos. 26 (2005) 60–65.

[10] C. Yan, L. Liu, Y. Zhu, H. Xu, D. Liu, Properties of polymerized cyclic butylene terephthalate and its composites via ring-opening polymerization, J. Thermoplast. Compos. Mater. 31 (2018) 181–201, https://doi.org/10.1177/0892705711697774.

[11] C.M. Ó Brádaigh, A. Doyle, D. Doyle, P. Feerick, Electrically-heated ceramic composite tooling for out-of-autoclave manufacturing of large composite structures, SAMPE J. 47 (2011) 6–14http://hdl.handle.net/10379/3542, Accessed date: 1 January 2019.

[12] A. Doyle, P. Feerick, P. Mallon, C. Ó Brádaigh, D. Doyle, A heated mould for moulding polymeric composites, a method for making such mould and its use, European Patent EP (2012) 2344312B1http://www.freepatentsonline.com/WO2010040576.html, Accessed date: 1 January 2019.

[13] G. Gardiner, Thermoplastic Wind Blades: To be or not? 2012 https://www.compositesworld.com/articles/thermoplastic-wind-blades-to-be-or-not (accessed January 1, 2019).

[14] R.E. Murray, D. Snowberg, D. Berry, R. Beach, S. Rooney, D. Swan, Manufacturing a 9-meter thermoplastic composite wind turbine blade, Am. Soc. Compos. 32nd Tech. Conf., West Lafayette, Indiana, 2017www.nrel.gov/publications, Accessed date: 1 January 2019.

[15] D.S. Cousins, Y. Suzuki, R.E. Murray, J.R. Samaniuk, A.P. Stebner, Recycling glass fiber thermoplastic composites from wind turbine blades, J. Clean. Prod. 209 (2019) 1252–1263, https://doi.org/10.1016/j.jclepro.2018.10.286.

[16] C. Baley, M. Lan, A. Bourmaud, A. Le Duigou, Compressive and tensile behaviour of unidirectional composites reinforced by natural fibres: influence of fibres (flax and jute), matrix and fibre volume fraction, Mater. Today Commun. 16 (2018) 300–306, https://doi.org/10.1016/j.mtcomm.2018.07.003.

[17] A. Aronica, D. Fossati, Effects of Resin and Processing on Mechanical Properties of Carbon Fibre Composites, Politecnico di Milano, 2015 Master's Thesis.

[18] T. Pini, F. Caimmi, F. Briatico-Vangosa, R. Frassine, M. Rink, Fracture initiation and propagation in unidirectional CF composites based on thermoplastic acrylic resins, Eng. Fract. Mech. 184 (2017) 51–58, https://doi.org/10.1016/j.engfracmech.2017.08.023.

[19] T. Pini, F. Briatico-Vangosa, R. Frassine, M. Rink, Matrix toughness transfer and fibre bridging laws in acrylic resin based CF composites, Eng. Fract. Mech. 203 (2018) 115–125, https://doi.org/10.1016/j.engfracmech.2018.03.026.

[20] T. Pini, F. Briatico-Vangosa, R. Frassine, M. Rink, Time dependent fracture behaviour of a carbon fibre composite based on a (rubber toughened) acrylic polymer, Procedia Struct. Integr. 2 (2016) 253–260, https://doi.org/10.1016/j.prostr.2016.06.033.

[21] A. Aronica, D. Fossati, Mechanical Properties of Carbon Fiber Composite Materials, Politecnico di Milano, 2014 [Master's Thesis].

[22] A. Monti, A. El Mahi, Z. Jendli, L. Guillaumat, Mechanical behaviour and damage mechanisms analysis of a flax-fibre reinforced composite by acoustic emission, Compos. Part A Appl. Sci. Manuf. 90 (2016) 100–110, https://doi.org/10.1016/j.compositesa.2016.07.002.

[23] P. Davies, M. Arhant, Fatigue behaviour of acrylic matrix composites: influence of seawater, Appl. Compos. Mater. (2018) 1–12, https://doi.org/10.1007/s10443-018-9713-1.

[24] A. Chilali, W. Zouari, M. Assarar, H. Kebir, R. Ayad, Analysis of the mechanical behaviour of flax and glass fabrics-reinforced thermoplastic and thermoset resins, J. Reinf. Plast. Compos. 35 (2016) 1217–1232, https://doi.org/10.1177/0731684416645203.

[25] S.K. Bhudolia, P. Perrotey, S.C. Joshi, Optimizing polymer infusion process for thin ply textile composites with novel matrix system, Materials (Basel) 10 (2017)https://doi.org/10.3390/ma10030293.

[26] M.R. Boumbimba, M. Coulibaly, A. Khabouchi, G. Kinvi-Dossou, N. Bonfoh, P. Gerard, Glass fibres reinforced acrylic thermoplastic resin-based tri-block copolymers composites: low velocity impact response at various temperatures, Compos. Struct. 160 (2017) 939–951, https://doi.org/10.1016/j.compstruct.2016.10.127.

[27] S.K. Bhudolia, S.C. Joshi, Low-velocity impact response of carbon fibre composites with novel liquid methylmethacrylate thermoplastic matrix, Compos. Struct. 203 (2018) 696–708, https://doi.org/10.1016/j.compstruct.2018.07.066.

[28] G. Kinvi-Dossou, R. Matadi Boumbimba, N. Bonfoh, S. Garzon-Hernandez, D. Garcia-Gonzalez, P. Gerard, A. Arias, Innovative acrylic thermoplastic composites versus conventional composites: improving the impact performances, Compos. Struct. 217 (2019) 1–13, https://doi.org/10.1016/j.compstruct.2019.02.090.

[29] W. Obande, D. Ray, C.M. Ó Brádaigh, Viscoelastic and drop-weight impact properties of an acrylic-matrix composite and a conventional thermoset composite – a comparative study, Mater. Lett. 238 (2019) 38–41, https://doi.org/10.1016/j.matlet.2018.11.137.

[30] S.K. Bhudolia, P. Perrotey, S.C. Joshi, Mode I fracture toughness and fractographic investigation of carbon fibre composites with liquid methylmethacrylate thermoplastic matrix, Compos. Part B Eng. 134 (2018) 246–253, https://doi.org/10.1016/j.compositesb.2017.09.057.

[31] M. Haggui, A. El Mahi, Z. Jendli, A. Akrout, M. Haddar, Damage analysis of flax fibre/elium composite under static and fatigue testing, in: M. Haddar, F. Chaari, A. Benamara, M. Chouchane, C. Karra, N. Aifaoui (Eds.), Des. Model. Mech. Syst, Springer International Publishing, Cham 2018, pp. 681–691.

[32] M. Haggui, A. El Mahi, Z. Jendli, A. Akrout, M. Haddar, Static and fatigue characterization of flax fiber reinforced thermoplastic composites by acoustic emission, Appl. Acoust. 147 (2019) 100–110, https://doi.org/10.1016/j.apacoust.2018.03.011.

[33] P. Davies, Environmental degradation of composites for marine structures: new materials and new applications, Philos. Trans. R. Soc. A Math. Phys. Eng. Sci. 374 (2016) 1–14 (doi:ARTN 20150272\r10.1098/rsta.2015.0272).

[34] P. Davies, P.-Y. Le Gac, M. Le Gall, M. Arhant, Marine ageing behaviour of new environmentally friendly composites, in: P. Davies, Y.D.S. Rajapakse (Eds.), Durab. Compos. a Mar. Environ, vol. 2, Springer International Publishing, Cham 2018, pp. 225–237, https://doi.org/10.1007/978-3-319-65145-3_12.

[35] L. Freund, V. Bouchart, H. Perrin, P. Chevrier, Hydrothermal aging of natural fibers composite: determination of diffusivity parameters, ECCM17 - 17th Eur. Conf. Compos. Mater, 2016.

[36] A. Chilali, W. Zouari, M. Assarar, H. Kebir, R. Ayad, Effect of water ageing on the load-unload cyclic behaviour of flax fibre-reinforced thermoplastic and thermosetting composites, Compos. Struct. 183 (2018) 309–319, https://doi.org/10.1016/j.compstruct.2017.03.077.

[37] A. Chilali, M. Assarar, W. Zouari, H. Kebir, R. Ayad, Effect of geometric dimensions and fibre orientation on 3D moisture diffusion in flax fibre reinforced thermoplastic and thermosetting composites, Compos. Part A Appl. Sci. Manuf. 95 (2017) 75–86, https://doi.org/10.1016/j.compositesa.2016.12.020.

[38] J. Beguinel, J.-F. Gérard, F. Lortie, P. Gérard, J. Maupetit, New continuous fiber reinforced thermoplastic composites: an analysis of interfacial adhesion from the micro scale to the macro scale, 20th Int. Conf. Compos. Mater, 2015.

[39] Z. Boufaida, L. Farge, S. André, Y. Meshaka, Influence of the fiber/matrix strength on the mechanical properties of a glass fiber/thermoplastic-matrix plain weave fabric composite, Compos. Part A Appl. Sci. Manuf. 75 (2015) 28–38, https://doi.org/10.1016/j.compositesa.2015.04.012.

[40] T. Pini, F. Briatico-Vangosa, R. Frassine, M. Rink, Fracture toughness of acrylic resins: viscoelastic effects and deformation mechanisms, Polym. Eng. Sci. 58 (2018) 369–376, https://doi.org/10.1002/pen.24583.

[41] T. Pini, Fracture Behaviour of Thermoplastic Acrylic Resins and Their Relevant Unidirectional Carbon Fibre Composites: Rate and Temperature Effects, Politecnico di Milano, 2017 [Doctoral Thesis].

[42] M. Haggui, Z. Jendli, A. Akrout, A. El Mahi, Damage identification in flax fibre composite with thermoplastic matrix under quasi-static loading, Int. Conf. Adv. Mater. Mech. Manuf 2016, pp. 1–4.

[43] M. Haggui, A. El Mahi, Z. Jendli, A. Akrout, Damage characterization of flax fibre composite using linear and nonlinear vibration resonant techniques, 26th Annu. Int. Conf. Compos. Eng, 2018.

[44] Q. Lin, M. Ferriol, M. Cochez, H. Vahabi, C. Vagner, Continuous fiber-reinforced thermoplastic composites: influence of processing on fire retardant properties, Fire Mater 41 (2017) 646–653, https://doi.org/10.1002/fam.2406.

[45] S.K. Bhudolia, P. Perrotey, S.C. Joshi, Enhanced vibration damping and dynamic mechanical characteristics of composites with novel pseudo-thermoset matrix system, Compos. Struct. 179 (2017) 502–513, https://doi.org/10.1016/j.compstruct.2017.07.093.

[46] G. Fredi, A. Dorigato, A. Pegoretti, Novel reactive thermoplastic resin as a matrix for laminates containing phase change microcapsules, Polym. Compos. (2019)https://doi.org/10.1002/pc.25233.

[47] T. Lorriot, J. El Yagoubi, J. Fourel, F. Tison, Non-conventional glass fiber NCF composites with thermoset and thermoplastic matrices, 20th Int. Conf. Compos. Mater., Copenhagen, 2015https://www.researchgate.net/publication/301684388, Accessed date: 17 January 2019.

[48] D.S. Cousins, Advanced Thermoplastic Composites for Wind Turbine Blade Manufacturing, Colorado School of Mines, 2018 [Doctoral Thesis].

[49] P. Davies, P.Y. Le Gac, M. Le Gall, Influence of sea water aging on the mechanical behaviour of acrylic matrix composites, Appl. Compos. Mater. 24 (2017) 97–111, https://doi.org/10.1007/s10443-016-9516-1.

[50] R.E. Murray, D. Penumadu, D. Cousins, R. Beach, D. Snowberg, D. Berry, Y. Suzuki, A. Stebner, Manufacturing and flexural characterization of infusion-reacted thermoplastic wind turbine blade subcomponents, Appl. Compos. Mater. 27 (2019) 1–17, https://doi.org/10.1007/s10443-019-9760-2.

[51] D. Zhang, A.M. Waas, C.-F. Yen, Progressive damage and failure response of hybrid 3D textile composites subjected to flexural loading, part I: experimental studies, Int. J. Solids Struct. 75–79 (2015) 309–320, https://doi.org/10.1016/j.ijsolstr.2015.06.034.

[52] M.J. Hiley, Fractographic study of static and fatigue failures in polymer composites Fractographic study of static and fatigue failures in polymer composites, Plast. Tubber Compos. 28 (1999) 210–227, https://doi.org/10.1179/146580199101540358.

[53] F.A. Almansour, H.N. Dhakal, Z.Y. Zhang, Effect of water absorption on mode I interlaminar fracture toughness of flax/basalt reinforced vinyl ester hybrid composites, Compos. Struct. 168 (2017) 813–825, https://doi.org/10.1016/j.compstruct.2017.02.081.

[54] F. Bensadoun, I. Verpoest, A.W. Van Vuure, Interlaminar fracture toughness of flax-epoxy composites, J. Reinf. Plast. Compos. 36 (2017) 121–136, https://doi.org/10.1177/0731684416672925.

[55] T. Eliades, S. Zinelis, D. Kim, W. Brantley, Structure/property relationships in orthodontic polymers, Orthod. Appl. Biomater 2017, pp. 39–59, https://doi.org/10.1016/B978-0-08-100383-1.00002-3.

[56] M. Sudheer, Thermomechanical properties of epoxy/PTW composites, J. Mech. Eng. Autom. 6 (2016) 18–21, https://doi.org/10.5923/c.jmea.201601.04.

[57] V. Chaudhari, H. Chandekar, J. Saboo, A. Mascarenhas, Studies on thermo-mechanical properties of chemically treated jute-polyester composite, IOP Conf. Ser. Mater. Sci. Eng, vol. 330, 2018, pp. 1–9, https://doi.org/10.1088/1757-899X/330/1/012032.

[58] A. Mousa, G. Heinrich, U. Wagenknecht, Wood-like material from thermoplastic polymer and landfill bio-materials: DMA, TGA and solvent resistance properties, Polym. from Renew. Resour. 6 (2015) 25–42 http://www.polymerjournals.com/pdfdownload/1189819.pdf (accessed April 29, 2019).

[59] K. Bandzierz, L. Reuvekamp, J. Dryzek, W. Dierkes, A. Blume, D. Bielinski, , Influence of network structure on glass transition temperature of elastomers Materials (Basel) 9 (2016) 1–17, https://doi.org/10.3390/MA9070607.